Role of Activated Chemisorption in Gas-Mediated Electron Beam Induced Deposition

James Bishop, Charlene J. Lobo, Aiden Martin, Mike Ford, Matthew Phillips, and Milos Toth*

School of Physics and Advanced Materials, University of Technology, Sydney, P.O. Box 123, Broadway, New South Wales 2007, Australia

(Received 18 July 2012; revised manuscript received 13 August 2012; published 3 October 2012)

Models of adsorbate dissociation by energetic electrons are generalized to account for activated sticking and chemisorption, and used to simulate the rate kinetics of electron beam induced chemical vapor deposition (EBID). The model predicts a novel temperature dependence caused by thermal transitions from physisorbed to chemisorbed states that govern adsorbate coverage and EBID rates at elevated temperatures. We verify these results by experiments that also show how EBID can be used to deposit high purity materials and characterize the rates and energy barriers that govern adsorption.

DOI: 10.1103/PhysRevLett.109.146103 PACS numbers: 68.43.Mn, 81.07.−b, 81.15.Dj, 82.30.Lp

Electron beam induced deposition (EBID) and etching (EBIE) entail electron dissociation of precursor adsorbates into fragments that react with a solid surface [1–4]. Etching is caused by fragments that react with surface molecules to form volatile species which desorb, thereby removing surface material. Deposition occurs when the reaction products are nonvolatile, resulting in the addition of surface material comprised of precursor molecule constituents. EBID is typically performed at or close to room temperature by injecting a precursor gas into a high or ultrahigh vacuum electron microscope while a substrate is irradiated by an energetic ($\sim$ 1–300 keV) electron beam. EBID and EBIE growth kinetics are modeled by rate equations that account for precursor transport, adsorption, desorption, surface diffusion, and electron dissociation rates [3–5]. However, to date, only adsorption into a single physisorbed state has been considered. Chemisorption is known to play a role [1–4,6], but has been neglected in models of rate kinetics. This is in part because it is undesirable if it causes delocalized processing in the absence of electron irradiation [3], as in the spontaneous etching of Si by XeF_2 [7].

Here we present a model of EBID rate kinetics that accounts for activated (as well as spontaneous) chemisorption [8], is applicable to both EBID and EBIE, and reduces to existing models [2,4,5] in the absence of chemisorbed surface states. It yields the correct, well known temperature dependence of EBID in the absence of chemisorption [4], and reveals novel behavior arising from thermally activated transitions from physisorbed to chemisorbed states that dominate precursor coverage and give rise to high EBID rates and material purity at elevated temperature. The model is verified by measuring EBID rates and the elemental composition of deposits grown with a tetraethoxysilane (TEOS) precursor versus substrate temperature.

In the limit of low electron flux [9] EBID is described by Refs. [2,4,5]

$$\frac{\partial N_p}{\partial t} = s_p F \Lambda_p - N_p(k_p + \sigma_p f), \tag{1}$$

$$\frac{\partial N}{\partial t} = N_p \sigma_p f. \tag{2}$$

Equation (1) is the rate of change of the physisorbed species concentration N_p, and Eq. (2) is the deposition rate per unit area (molecules/ Å^2/ s). Equation (1) is a sum of fluxes (molecules/Å^2/ s) representing precursor molecule arrival into the physisorbed state from the gas phase through adsorption $s_p F \Lambda_p$, adsorbate removal through desorption $-N_p k_p$, and conversion of the adsorbates to a deposit through electron induced dissociation $-N_p \sigma_p f$. In these equations, N_p and N are the concentrations of physisorbed and dissociated precursor molecules at the surface (Å^{-2}), s_p is the sticking coefficient, F is the gas molecule flux at the surface (Å^{-2} s^{-1}), and Λ_p is the fraction of unoccupied surface sites available for physisorption. The desorption and dissociation rates of the physisorbed species are k_p and $\sigma_p f$ (molecules per s), where σ_p is the effective cross section [10] for electron dissociation of physisorbed molecules (Å^{-2}) and f is the electron flux at the surface (Å^{-2}s^{-1}).

The gas flux is given by $F = P/(2\pi m_g k T_g)^{1/2}$, where k is Boltzmann's constant, and m_g, P, and T_g are the gas molecule mass, gas pressure, and temperature, respectively. The sticking coefficient s_p is the fraction of incident gas molecules that scatter with the surface inelastically and are trapped in the physisorption potential well. Surface site occupation is typically limited to one monolayer by the Langmuir isotherm ($\Lambda_p = 1 - A_p N_p$, where A_p is the area of a single site), and the desorption rate k_p is defined by the energy barrier for desorption into the gas phase, E_d, and the prefactor κ_p

$$k_p = 1/\tau_p = \kappa_p e^{-E_d/kT}, \tag{3}$$

where T is the temperature of the surface (as opposed to the gas temperature, T_g).

A surface with chemisorbed and physisorbed states characterized by binding energies E_D and E_d, and

separated by an energy barrier E_c can be represented by the reaction coordinate diagram shown in Fig. 1 [8]. Chemisorption from the gas phase is activated if $E_c > E_d$, as shown in the figure. Chemisorption can be incorporated in the standard EBID model [Eqs. (1) and (2)] by accounting for the rate of change of the concentration of chemisorbed molecules, $\partial N_c/\partial t$, caused by transitions between the gas phase, physisorbed and chemisorbed states shown in Fig. 1, and by enabling electron dissociation of the chemisorbed species [9]:

$$\frac{\partial N_p}{\partial t} = s_p(1 - s_c)F\Lambda_p - N_p(k_p + k_c\Lambda_c + \sigma_p f), \quad (4)$$

$$\frac{\partial N_c}{\partial t} = n(s_c F + N_p k_c)\Lambda_c - N_c(k_D + \sigma_c f), \quad (5)$$

$$\frac{\partial N}{\partial t} = f(N_p\sigma_p + N_c\sigma_c). \quad (6)$$

In the above, s_c is the sticking coefficient for thermally activated chemisorption from a gas at temperature T_g [8], defined by the barrier $(E_c - E_d)$ and the preexponential factor s_0

$$s_c = s_0 e^{-(E_c - E_d)/kT_g}. \quad (7)$$

Equation (4) is analogous to Eq. (1), but the physisorption term $s_p(1 - s_c)F\Lambda_p$ excludes gas molecules that have sufficient thermal energy kT_g in the gas phase to surmount the activation barrier $(E_c - E_d)$ and become trapped directly in the chemisorbed state [11]. The term $N_p k_c \Lambda_c$ is the flux of molecules that transition from the physisorbed to the chemisorbed state by gaining thermal energy kT from the surface, and n is the number of surface sites occupied by each chemisorbed molecule. This is the dominant activated chemisorption pathway when EBID is performed using a heated substrate and the electron microscope chamber and gas delivery system are not heated so that T_g remains close to room temperature.

Λ_c is the fraction of unoccupied surface sites available for chemisorption (limited to one monolayer: $\Lambda_c = 1 - A_c N_c$), and σ_c is the effective cross section [10] for electron induced dissociation of chemisorbed molecules. The rate coefficients for conversion of adsorbates from the physisorbed to the chemisorbed state, k_c, and desorption of chemisorbed adsorbates, k_D, are governed by the substrate temperature and are given by

$$k_c = \kappa_c e^{-E_c/kT}, \quad (8)$$

$$k_D = \kappa_D e^{-E_D/kT}, \quad (9)$$

where κ_c and κ_D are the relevant prefactors.

Equations (4)–(6) are solved to yield the concentrations of physisorbed and chemisorbed species and the EBID (or EBIE) rate, which is proportional to $\partial N/\partial t$. The latter is the sum of two fluxes corresponding to dissociation of physisorbed $(N_p\sigma_p f)$ and chemisorbed $(N_c\sigma_c f)$ adsorbates.

The dependence of $\partial N/\partial t$ on substrate temperature that is applicable to EBID is shown in Fig. 2 (calculated using the model input parameters discussed below). The physisorption component $N_p\sigma_p f$ decreases with T due to an increase in the thermal desorption rate k_p [Eq. (3)], and a corresponding decrease in N_p. This behavior is characteristic of standard EBID models [4,5]. Conversely, the chemisorption component, $N_c\sigma_c f$, is negligible at room temperature [N_c is low as $(E_c - E_d) \gg kT$]. It exhibits an increase followed by a decrease with T as the surface temperature becomes sufficiently high to enable efficient adsorbate conversion from the physisorbed to the chemisorbed state [Eq. (8)] and desorption from the chemisorbed state [Eq. (9)], respectively. The general temperature dependence seen in Fig. 2 (i.e., a decrease followed by a peak in $\partial N/\partial t$) exists only if $k_p \ll k_c \ll k_D$.

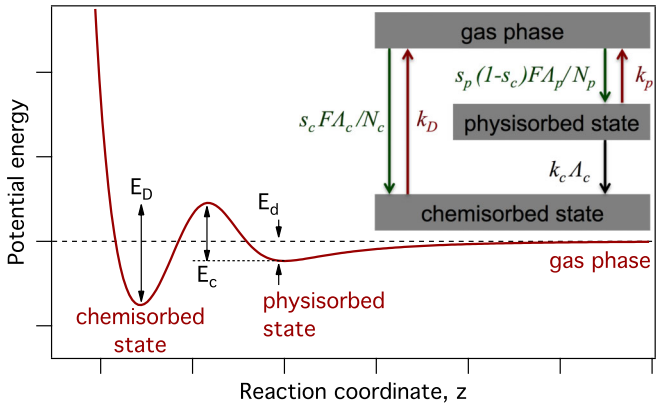

FIG. 1 (color online). Schematic one-dimensional potential energy diagram for physisorption and activated chemisorption (z = distance above the surface). *Inset:* Transition rates [molecules/s] between the gas phase, physisorbed state, and chemisorbed state.

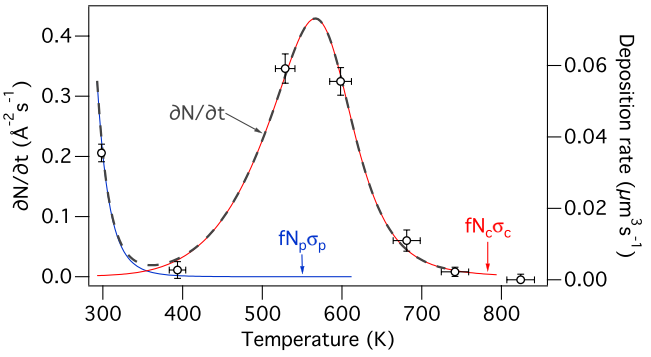

FIG. 2 (color online). Steady state adsorbate dissociation rates calculated using Eqs. (4)–(6) as a function of substrate temperature, and the corresponding deposition rates measured using tetraethoxysilane precursor (∘).

The behavior predicted by Eqs. (4)–(6) was verified experimentally using TEOS, a precursor used for the deposition of SiO_2, and Si (111) substrates with a native oxide layer. On amorphous SiO_2 surfaces, TEOS physisorbs at room temperature, chemisorbs at ~450 K and decomposes to form SiO_2 at temperatures greater than ~800 K [12,13]. EBID experiments were carried out using a FEI XL30 environmental scanning electron microscope (ESEM) [14] with a thermionic tungsten hairpin electron source. The ESEM specimen chamber was modified to house a variable pressure subchamber described previously [15] that enables the use of EBID precursor gases while maintaining the enclosing specimen chamber under vacuum. The subchamber contains a capacitance manometer, sample holder, Faraday cup, heater, *K*-type thermocouples, and a gas cascade electron detector [16]. The detector signal [17], pressure, and sample, and cell wall temperatures were recorded as a function of time during EBID. After pumping of the ESEM and the subchamber to a base pressure of $\sim 10^{-4}$ Pa, TEOS was introduced into the subchamber and maintained at a pressure of 6.7 Pa using a pressure-feedback gas delivery system [18]. The electron beam was admitted to the substrate through a 200 μm pressure limiting aperture [14] located between the subchamber and a differentially pumped electron column.

EBID was performed using a 25 keV electron beam with a diameter of 1.5 μm configured to yield a top-hat flux profile [19] with a peak flux of 80 electrons/Å^2/s. The deposition rates plotted in Fig. 2 were obtained by dividing the volume of deposits grown using a stationary beam (see, for example, Ref. [19]) by the growth time of 1800 s at each substrate temperature T. The vertical error bars in Fig. 2 account for beam current drift, distortions in deposit geometry caused by electrons emitted from sidewalls, and errors in volumes measured from top-down and high tilt (~ 90°) electron images. Uncertainties in T account for differences between temperatures measured at the sample surface and the support, and thermal drift that occurred during deposition.

Qualitatively, the experimental growth rates in Fig. 2 are in excellent agreement with the temperature dependence predicted by Eqs. (4)–(6). Significantly, the experiments show the peak in the EBID growth rate expected from thermally activated chemisorption. The quantitative modeling data in Fig. 2 were obtained by solving Eqs. (4)–(6) numerically under steady state conditions so as to yield the equilibrium concentrations of physisorbed and chemisorbed adsorbates, and the corresponding deposition rates. The experimental EBID gas pressure and electron flux conditions were used as model input parameters, and molecular parameters were estimated based on prior experimental literature on adsorption on SiO_2 and thermal chemical vapor deposition (CVD) of TEOS [13,20–22]. The physisorbed and chemisorbed adsorbates on amorphous SiO_2 surfaces are known to be very similar. The physisorbed species is $Si(OC_2H_5)_4$ (TEOS), and the chemisorbed species is a mixture of $(SiO)_2Si(OC_2H_5)_2$ and $(SiO)Si(OC_2H_5)_3$ [12,13]. Because of the similarity between the physisorbed and chemisorbed adsorbates, the corresponding surface site areas were assumed to be equal at $A_p = A_c = 100$ Å^2. This equates to surface site densities of 10^{14} cm^{-2}, in good agreement with prior studies of adsorption on SiO_2 [22]. The dissociation cross sections were also assumed equal at $\sigma_p = \sigma_c = 10$ Å^2. The desorption and transition rate prefactors were set to $\kappa_p = \kappa_D = \kappa_c = 10^{15}$ s^{-1}, a value appropriate for large adsorbates [23]. The activation energies E_d, E_c, and E_D were varied to fit the experimental data in Fig. 2 [11].

Under electron irradiation, the calculated concentrations of both physisorbed and chemisorbed species reached a steady state within 0.1 s over the entire temperature range studied experimentally ($T_s \geq 300$ K). The values of the activation energies that gave the best fit to the experimental deposition rates were as follows: $E_d = 0.51$ eV, $E_c = 0.86$ eV, and $E_D = 1.42$ eV. These energies are reasonable given the prior experimental literature on TEOS adsorption on SiO_2 [12,13,20], and result in complete desorption of the physisorbed species by 400 K, and complete desorption of the chemisorbed species by 800 K, consistent with Tedder *et al.* [13].

We note that in the model, T_g was fixed at 300 K, whereas in the experiments the subchamber wall temperature increased up to ~350 K as the substrate was heated to ~800 K, due to radiative and convective heat transfer to the subchamber walls. T_g therefore increased with T, and may alter the chemisorption rate through Eq. (7). We find this effect to be insignificant under the experimental conditions used here, over any realistic range of T_g. This was investigated by simulations performed using a gas temperature $T_g = 300 + i(T - 300)$, where i was varied from 0 to 0.2. The resulting behavior, shown in Fig. 3, is not surprising given the high value of $(E_c - E_d)$ relative to the maximum value of kT_g.

Similarly, changes in s_0 and A_c had an insignificant effect on the results (also shown in Fig. 3). Hence, for the case of

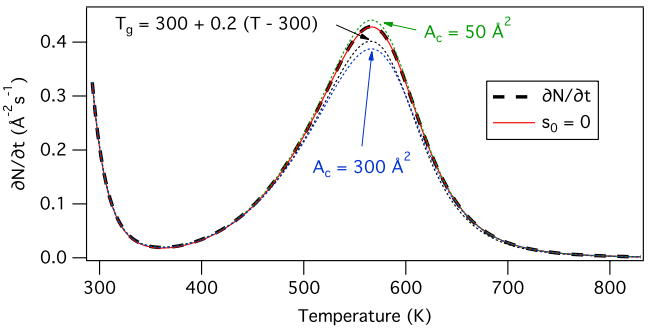

FIG. 3 (color online). Steady state adsorbate dissociation rate ($\partial N/\partial t$) calculated using the model input parameters in the text, and recalculated using $s_0 = 0$, $A_c = 50$ Å^2, $A_c = 300$ Å^2, and $T_g = 300 + 0.2(T - 300)$.

cold-wall TEOS-mediated EBID, direct chemisorption from the gas phase is negligible ($s_c \sim 0$), and dissociative chemisorption can be approximated by an expression for a single chemisorbed species, as in Eq. (5), rather than requiring individual equations for each fragment species chemisorbed at the surface.

The validity of this model is substantiated further by measurements of the deposit composition at each temperature. Elemental composition was determined by energy dispersive x-ray spectroscopy [24] (performed at room temperature, using a 5 keV electron beam, in the absence of a TEOS precursor), which measures the characteristic x-ray spectrum from the sample region probed by the electron beam. Line scans were taken across each deposit, and the data analyzed to extract the carbon-to-oxygen K_α x-ray peak ratio as a function of substrate temperature used during EBID. Below 400 K, where EBID results from dissociation of physisorbed TEOS molecules, the average C/O ratio at the center of each deposit is ~0.25. Above 400 K, where EBID is attributed to chemisorbed adsorbates, the average C/O ratio is also constant, but has a much lower value of ~0.05. This correlation between a dramatic increase in growth rate (Fig. 2) and a large reduction in carbon content is indicative of electron-induced dissociation of different adsorbate species in each temperature regime, and efficient desorption of carbon-containing fragments at elevated temperatures.

The high impurity content of deposits grown near room temperature is typical of TEOS EBID [25], and of EBID in general [2–4,26]. Unlike electron induced dissociation performed inside a scanning tunneling microscope [27], the EBID process is not bond selective, as it entails the use of electrons with a wide energy spectrum [10] that can break all bonds within an adsorbate [4]. Most EBID precursors have organic ligands [1–4,26], so this often results in deposits with high carbon content (e.g., >50 at. %). Substrate heating has been reported to improve deposit purity, but this improvement has been accompanied by reduced EBID rates (due to thermal depopulation of physisorbed surface states) or by delocalized film growth caused by thermal CVD [28]. In contrast, the results presented here show that precursors that undergo thermally activated chemisorption enable both high EBID rates and deposit purity to be realized in the absence of delocalized thermal growth.

This work was funded by FEI Company and The Australian Research Council.

*Milos.Toth@uts.edu.au

[1] S. J. Randolph, J. D. Fowlkes, and P. D. Rack, Crit. Rev. Solid State Mater. Sci. **31**, 55 (2006).
[2] W. F. van Dorp and C. W. Hagen, J. Appl. Phys. **104**, 081301 (2008).
[3] I. Utke, P. Hoffmann, and J. Melngailis, J. Vac. Sci. Technol. B **26**, 1197 (2008).
[4] I. Utke, S. Moshkalev, and P. Russell, *Nanofabrication Using Focused Ion and Electron Beams: Principles and Applications* (Oxford University, New York, 2012).
[5] S. Randolph, M. Toth, J. Cullen, C. Chandler, and C. Lobo, Appl. Phys. Lett. **99**, 213103 (2011).
[6] O. Guise, H. Marbach, J. Levy, J. Ahner, and J. T. Yates, Surf. Sci. **571**, 128 (2004).
[7] R. C. Hefty, J. R. Holt, M. R. Tate, D. B. Gosalvez, M. F. Bertino, and S. T. Ceyer, Phys. Rev. Lett. **92**, 188302 (2004).
[8] G. Ehrlich, J. Phys. Chem. **59**, 473 (1955); S. G. Brass and G. Ehrlich, Phys. Rev. Lett. **57**, 2532 (1986).
[9] For clarity, we omit surface diffusion from the equations. Diffusion plays a role only if an adsorbate concentration gradient exists at the surface, and is negligible in the reaction rate limited regime of low electron flux [4,5].
[10] The effective cross sections σ_p and σ_c are weighed by the overlap between the corresponding energy dependent cross section and energy spectra of electrons incident onto and emitted from the substrate [4].
[11] In this general analysis, we ignore changes in activation energies encountered when chemisorption requires excitation of internal degrees of freedom, and nonlinear effects caused by adsorbate-adsorbate interactions [8].
[12] J. E. Crowell, L. L. Tedder, H. C. Cho, F. M. Cascarano, and M. A. Logan, J. Electron Spectrosc. Relat. Phenom. **54**, 1097 (1990); L. L. Tedder, J. E. Crowell, and M. A. Logan, J. Vac. Sci. Technol. A **9**, 1002 (1991).
[13] L. L. Tedder, G. Lu, and J. E. Crowell, J. Appl. Phys. **69**, 7037 (1991).
[14] G. D. Danilatos, Adv. Electron. Electron Phys. **71**, 109 (1988).
[15] C. J. Lobo, A. Martin, M. R. Phillips, and M. Toth, Nanotechnology **23**, 375302 (2012).
[16] M. Toth, M. Uncovsky, W. R. Knowles, and F. S. Baker, Appl. Phys. Lett. **91**, 053122 (2007).
[17] T. Bret, I. Utke, A. Bachmann, and P. Hoffmann, Appl. Phys. Lett. **83**, 4005 (2003).
[18] M. Toth, C. J. Lobo, W. R. Knowles, M. R. Phillips, M. T. Postek, and A. E. Vladar, Nano Lett. **7**, 525 (2007).
[19] J. Li, M. Toth, V. Tileli, K. A. Dunn, C. J. Lobo, and B. L. Thiel, Appl. Phys. Lett. **93**, 023130 (2008); J. T. Li, M. Toth, K. A. Dunn, and B. L. Thiel, J. Appl. Phys. **107**, 103540 (2010).
[20] S. C. Deshmukh and E. S. Aydil, J. Vac. Sci. Technol. A **13**, 2355 (1995).
[21] J. B. Danner and J. M. Vohs, Langmuir **10**, 3116 (1994); T. Luts and A. Katz, Top. Catal. **55**, 84 (2012).
[22] G. Cartry, L. Magne, and G. Cernogora, J. Phys. D **33**, 1303 (2000).
[23] K. A. Fichthorn and R. A. Miron, Phys. Rev. Lett. **89**, 196103 (2002).
[24] D. E. Newbury, D. C. Joy, P. Echlin, C. Fiori, and J. Goldstein, *Advanced Scanning Electron Microscopy and X-Ray Microanalysis* (Springer, New York, 1986).
[25] A. Perentes and P. Hoffmann, Chem. Vap. Deposition **13**, 176 (2007).
[26] A. Botman, J. J. L. Mulders, and C. W. Hagen, Nanotechnology **20**, 372001 (2009).
[27] S. Sakulsermsuk, P. A. Sloan, and R. E. Palmer, ACS Nano **4**, 7344 (2010).
[28] J. J. L. Mulders, L. M. Belova, and A. Riazanova, Nanotechnology **22**, 055302 (2011).